The Endothelium-Derived Hyperpolarizing Factor, H_2O_2, Promotes Metal-Ion Efflux in Aortic Endothelial Cells: Elemental Mapping by a Hard X-ray Microprobe†

Paul K. Witting,*,‡ Hugh H. Harris,§ Benjamin S. Rayner,‡ Jade B. Aitken,§ Carolyn T. Dillon,§,|| Roland Stocker,⊥ Barry Lai,@ Zhonghou Cai,@ and Peter A. Lay*,§

Vascular Biology Group, ANZAC Research Institute, Hospital Road, Concord Repatriation General Hospital, Concord, NSW 2139, Australia, Centre for Heavy Metal Research, School of Chemistry, The University of Sydney, Sydney, NSW 2006, Australia, Australian Key Centre for Microscopy and Microanalysis, Electron Microscope Unit, The University of Sydney, Sydney, NSW 2006, Australia, Centre for Vascular Research, School of Medical Sciences, University of New South Wales, Sydney, NSW 2052, Australia, and Experimental Facilities Division, Argonne National Laboratory, Argonne, Illinois 60439

Received March 4, 2006; Revised Manuscript Received May 28, 2006

ABSTRACT: Hydrogen peroxide (H_2O_2) is a physiologic oxidant implicated in vascular cell signaling, although little is known about the biochemical consequences of its reaction with endothelial cells. Submicrometer-resolution hard X-ray elemental mapping of cultured porcine aortic endothelial cells (PAEC) has provided data on the global changes for intracellular elemental density within PAEC and indicates an efflux of metal ions and phosphorus from the cytoplasm after H_2O_2 treatment. The synchrotron-radiation-induced X-ray emission experiments (SRIXE) show that H_2O_2-treated cells are irregularly shaped and exhibit blebbing indicative of increased permeability due to the damaged membrane. The SRIXE results suggest that H_2O_2-induced damage is largely restricted to the cell membrane as judged by the changes to membrane and cytoplasmic components rather than the cell nucleus. The SRIXE data also provide a mechanism for cell detoxification as the metal-ion efflux resulting from the initial H_2O_2-mediated changes to cell membrane potentially limits intracellular metal-mediated redox processes through Fenton-like chemistry. They may also explain the increased levels of these ions in atherosclerotic plaques, regardless of whether they are involved in plaque formation. Finally, the SRIXE data support the notion that cultured endothelial cells exposed to H_2O_2 respond with enhanced cellular metal-ion efflux into the extracellular space.

An intact and functional endothelium is vital for the maintenance of vascular homeostasis. It provides a physical barrier (*1*) to exclude circulating blood components from entering the sub-endothelial space, and endothelial cells synthesize and release a range of vaso-active factors. Chief among these factors is endothelium-derived nitric oxide ($^{\bullet}NO$)[1] produced through the action of nitric oxide synthase (eNOS) on L-arginine. Endothelium-derived $^{\bullet}NO$ is a mediator of vascular tone (*2*, *3*), regulates the interaction of platelets (*4*) and leukocytes (*5*) with the endothelium surface, and restricts vascular smooth muscle cell (VSMC) proliferation (*6*). The importance of $^{\bullet}NO$ in vascular homeostasis is emphasized by reports that an impaired endothelium-dependent arterial relaxation (termed endothelial dysfunction) predicts the occurrence of vascular disease (*7*). Moreover, diseases such as atherosclerosis (*8*), diabetes mellitus (*9*, *10*), and essential hypertension (*11*) are characterized by a dysfunctional endothelium that either is incapable of producing $^{\bullet}NO$ or does so with reduced $^{\bullet}NO$ bioavailability.

In addition to $^{\bullet}NO$, the endothelium produces an endothelium-derived hyperpolarizing factor (EDHF), the identity of which remains unclear. Candidates for this EDHF include hydrogen peroxide (H_2O_2) (*12*), cytochrome P450-derived epoxyeicosatrienoic acids (*13*), and endothelium-derived potassium ions (*14*). Of these, H_2O_2 is increasingly viewed

† This research was supported by the Australian Synchrotron Research Program (ASRP), which is funded by the Commonwealth of Australia under the Major National Research Facilities Program. The use of the Advanced Photon Source was supported by the U.S. Department of Energy, Office of Science, under Contract W-31-109-Eng-38. The research was also supported by the Australian Research Council (Research Fellowship DP034325 to P.K.W. and Discovery Grant DP0346162 and Professorial Fellowship DP0208409 to P.A.L.), an ASRP Fellowship to H.H.H., and the NHMRC of Australia (Senior Principal Research Fellowship 151602 to R.S.).

* To whom correspondence should be addressed: Centre for Heavy Metal Research, School of Chemistry, The University of Sydney, Sydney, NSW 2006, Australia. Phone: 61-2-9351-4269. Fax: 61-2-9351-3329. E-mail: p.lay@chem.usyd.edu.au.

‡ ANZAC Research Institute, Concord Repatriation General Hospital.

§ Centre for Heavy Metal Research, School of Chemistry, The University of Sydney.

|| Australian Key Centre for Microscopy and Microanalysis, Electron Microscope Unit, The University of Sydney. Current address: Department of Chemistry, University of Wollongong, Wollongong, NSW 2522, Australia.

⊥ University of New South Wales.

@ Argonne National Laboratory.

[1] Abbreviations: EDHF, endothelium-derived hyperpolarizing factor; eNOS, nitric oxide synthase; GFAAS, graphite-furnace atomic absorption spectroscopy; GSH, reduced glutathione; GSSG, glutathione disulfide; PAEC, porcine aortic endothelial cells; sGC, soluble guanylyl cyclase; SOD, superoxide dismutase; $O_2^{\bullet-}$, superoxide anion radical; SRIXE, synchrotron-radiation-induced X-ray emission; VSMC, vascular smooth muscle cells.

10.1021/bi0604375 CCC: $33.50
Published on Web 09/23/2006

as an important modulator of cellular events relevant to vascular function. Interestingly, H_2O_2 produced from the dismutation of superoxide anion radical ($O_2^{\bullet-}$) and independent of eNOS (*15*) acts as a signaling molecule (*16*), enhances endothelial $^{\bullet}NO$ production (*17*, *18*), modulates Ca^{2+}-ion (*19*) and K^+-ion (*20*) channel function, and inhibits VSMC growth (*21*).

Several sources of vascular H_2O_2 have been investigated, including $O_2^{\bullet-}$ produced by uncoupled eNOS (*22*), endothelial or plasma-derived xanthine oxidase (*23*), mitochondrial respiration (*24*), cytochrome P-450 (*25*), and both endothelial (*26*) and VSMC NAD(P)H oxidase (*27*). Notably, $O_2^{\bullet-}$ impairs $^{\bullet}NO$ bioactivity via the rapid formation of peroxynitrite (*28*). Peroxynitrite is capable of damaging eNOS directly (*29*) and indirectly (*30*) via oxidizing cofactors for eNOS.

The concentrations of H_2O_2 responsible for normal cell signaling are thought to be <1 μM (*31*), although pathologic concentrations of H_2O_2 can be significantly higher. For example, phorbol myristate acetate-activated blood leukocytes at a density of $1.5-6 \times 10^6$ cells/mL produce 0.08−0.48 mM H_2O_2 per hour (*32*), and enhanced H_2O_2 production is associated with diseases such as diabetes (*33*, *34*), hypertension (*35*), and atherosclerosis (*36*). Moreover, the EDHF effects of H_2O_2 in vitro are in the range of 10−100 μM (*12*). Despite this collective knowledge of the likely sources and concentration range of vascular H_2O_2, its apparent importance in the activation of Ca^{2+}- and K^+-ion channels, and its relation to hyperpolarization of VSMC, relatively little is known about the H_2O_2-induced global changes to the intracellular ion distribution in endothelial cells. Therefore, we have examined biochemical changes to cultured porcine aortic endothelial cells (PAEC) induced by a relatively low pathologic concentration of H_2O_2 (i.e., 50 μM) by using synchrotron-radiation-induced X-ray emission (SRIXE) mapping to directly assess the intracellular elemental distribution.

MATERIALS AND METHODS

Materials. HEPES buffer, trypsin (type III), L-glutamine, penicillin, streptomycin, fetal bovine serum (FBS), FLUO-3AM, and 30% (w/v) reagent H_2O_2 were obtained from Sigma. INDO-1 was purchased from Molecular Probes (Eugene, OR). M199 medium was purchased from JRH Biosciences (Lenexa, KS), and endothelial cell growth factor was purchased from Starrate Inc. (Sydney, Australia). An annexin V kit was obtained from BD Biosciences (San Diego, CA). Other chemicals were of the highest possible grade. Buffers were prepared with Millipore water and stored at 4 °C prior to use.

Cell Culture. Porcine aortic endothelial cells (PAEC) were obtained from Cell Applications (CA) and cultured in M199 medium supplemented with FBS (10%, v/v), 50 μg/mL heparin sulfate, 2 mm L-glutamine, 100 units/mL penicillin, and 100 μg/mL streptomycin at 37 °C and 5% CO_2(g), as described previously (*17*). Prior to use, confluent PAEC, between passages 3 and 6, were washed thoroughly with a HEPES-buffered physiologic salt solution (PSS) (*17*) and finally overlayed with HEPES-buffered PSS. The cells were then treated or not (vehicle alone control) with H_2O_2 at the final concentrations indicated in the figure legends. Treated and control PAEC were further incubated at 37 °C for 30 min, washed thoroughly with HEPES-buffered PSS, and harvested after being treated with trypsin to remove the adherent cells from the culture plate (*17*). Cell viability was assessed throughout by trypan blue exclusion assays, which showed that ~97% of control cells and ~95% of H_2O_2-treated cells remained viable after being harvested (not shown).

Preparation of Samples for SRIXE Analyses. Whole cell samples of PAEC were prepared as described previously (*37*, *38*). Treated and control PAEC (~10^6 cells) were thoroughly washed in phosphate buffer (50 mM, pH 7.4), harvested with 0.25% trypsin, and centrifuged, and the cell pellet was washed twice with phosphate-buffered saline (50 mM, pH 7.4, 150 mM NaCl). At this stage, cells were round in shape as assessed with a light microscope (10× magnification). Next, cells were transported to the School of Chemistry (The University of Sydney) in screw cap tubes placed in a plastic tube holder, embedded in ice, and prepared for use within 2 h of isolation. Briefly, the cells were pelleted; the buffer was exchanged with an ammonium acetate solution (200 mM, Ajax), and a sample of the resultant cell suspension (1.0 μL) was placed on Formvar films supported by 200 μm London Finder grids to allow the location of individual cells to be determined. The cells were flash-frozen in liquid nitrogen-cooled isopentane and then freeze-dried (24 h at −56 °C and 0.8 mbar). Cells were visualized on the Formvar grids with light microscopy before and after being freeze-dried and were macroscopically indistinguishable from cells immediately after being harvested with trypsin.

SRIXE Analysis. Hard X-ray microprobe experiments were performed on XOR beamline 2ID-D as described previously (*37*, *39*) using a monochromatic 10 keV X-ray incident beam, and a He atmosphere to eliminate the Ar K-shell fluorescence signal from air that masks the Cl and K signals. A number of fluorescence maps were collected simultaneously for each two-dimensional scan. Each map corresponded to the integrated Kα fluorescence signal of an element of interest. Elements routinely analyzed within each isolated cell were P, Cl, S, K, Ca, Cr, Fe, Cu, and Zn.

Briefly, whole cells were raster-scanned (using a 25 nm accuracy Newport positioning stage) with a beam focused to an ~0.3 μm diameter using a dual phase-zone-plate-based scanning hard X-ray microprobe (*40*). Individual cells on a gold TEM grid were located by phase-contrast microscopy. The grid markers were then imaged in the microprobe by collecting the X-ray transmission of the sample using a CCD camera placed behind a cadmium tungstate scintillator (*41*). This procedure centered on a single cell within a scan area of ~20 μm × 20 μm. SRIXE elemental distribution maps were acquired in fluorescence mode using 0.3 μm steps with a Canberra Ultra-LEGe single-element germanium detector with a sampling time of 3 s per point. The detector had an energy resolution of ~200 eV over the range of elements examined, and signal integration was performed during acquisition. An energy region for each characteristic Kα fluorescence peak was defined before data collection and corresponded approximately to the area under the full width at half-maximum of the peak. Elemental distribution maps were then normalized to the incident beam intensity, measured using an upstream N_2-filled ionization detector (I_0).

For SRIXE quantitation, the arbitrary total amount of each element investigated was determined as the area-integrated I_0-normalized fluorescence counts (within an energy region of interest with no background corrections), and this value was normalized to the cell volume of the identical cell employed in the SRIXE analyses (i.e., each volume was matched to the particular cell that was analyzed). Finally, the volume-normalized data obtained for control or H_2O_2-treated cells were averaged and expressed as means ± the standard deviation. Cell volumes were estimated by using the average of the maximum and minimum radii across each, presumed flattened, freeze-dried cell and extrapolating to three dimensions. While the amounts of individual elements can be compared between cells and treatments, it should be noted that the results are arbitrary in value and cannot be compared between elements, due to differing detection sensitivities, windows, and overlaps of peaks. The SRIXE results were not normalized against standards; however, absolute values for Fe, Cu, and Zn were obtained from the GFAAS results on bulk cells to calibrate the results. The mean cell radius obtained for PAEC was 7.1 ± 0.9 μm with a corresponding mean volume of 1500 ± 600 μm^3 ($n = 7$ cells across the different treatment groups). Color maps were generated using triangular connection interpolation and visualized with OpenDX (http://www.opendx.org).

Assessment of Intracellular Calcium by Flow Cytometry. The intracellular Ca^{2+} concentration was measured in cultured PAEC after H_2O_2 treatment by incubating with the fluorescent Ca^{2+}-chelating agents INDO-1 or FLUO-3AM (final probe concentration of ~2 μM) in HEPES-buffered PSS for 60 min followed by a 30 min incubation in the presence of media to de-esterify the probe as described previously (*42*). Finally, the PAEC were harvested and resuspended in PBS (50 mM, pH 7.4), and flow cytometry was performed with an LSR II FlowSystem or FACSCALIBUR cytometer (BD Sciences). Intracellular Ca^{2+} was quantified using a standard curve generated with a single concentration of the probe [dissociation constant $K_{d(Ca^{2+})}$ = 0.23 and 0.14 μM for INDO-1 and FLUO-3AM, respectively] dispersed in Ca^{2+}-free buffer by titrating with $CaCl_2$, as described previously (*42*). Where required, annexin V binding was employed as described by the manufacturer to measure the extent of apoptosis of PAEC exposed to H_2O_2; propidium iodide staining was employed as a measure of cell death. Flow cytometry was performed with a FASCALIBUR cytometer (BD Sciences).

Atomic Absorption Spectroscopy. Concentrations of Zn, Cu, and Fe in cultured PAEC were determined with graphite-furnace atomic absorbance spectroscopy (GFAAS) as described previously (*43*). Replicate experiments were performed and matched carefully to the protocol employed to generate samples designated for SRIXE. Thus, ~1−2 × 10^6 PAEC, with and without H_2O_2 pretreatment, were washed in phosphate buffer prepared with Milli-Q water that had been pretreated with Chelex100 to remove contaminating metals. Cells were harvested and centrifuged, and the cell pellet was initially stored in a fashion similar to that of samples employed in SRIXE analyses. At the appropriate time, the cells were lysed by repeated (three times) freeze−thaw cycles, and a sample (50 μL) from each of the lysates was removed for protein analyses. The remaining sample from control or H_2O_2-treated cells was diluted with concentrated nitric acid, incubated at 20 °C for 12 h, and then analyzed for Zn, Fe, and Cu content by GFAAS. The concentration of metal in the samples was then determined by comparison with a corresponding standard curve, and the absolute content of metal was normalized against the corresponding total cell protein for each individual sample after consideration for all dilution steps. Importantly, no change in cell protein was determined in either treatment group (not shown).

Electronic Absorbance Spectroscopy. The intracellular contents of reduced glutathione (GSH) and glutathione disulfide (GSSG), with and without H_2O_2 pretreatments, were determined with a commercial kit (Cayman Chemicals, Ann Arbor, MI). The cellular protein level was routinely measured using the BCA assay as instructed by the manufacturer (Sigma). Absorbance spectroscopy was performed using a multiwell plate reader (model 550, Bio-Rad).

Statistical Analysis. All data are expressed as means ± the standard deviation, and statistical analyses were performed using Prism (GraphPad, San Diego, CA). Mean data were from four control and three H_2O_2-treated cells. Many more cells were present on the grids, but time constraints on the beamline prohibited further analyses. The cells that were selected were those that did not overlap with other cells or were contaminated from any dust or other debris, as determined from optical microscopy. In addition, cells that were irregular in shape were also excluded for both control and H_2O_2-treated cells to reduce the likelihood of inclusion of cells in advanced stages of apoptosis or necrosis. The fact that the ratios of elements between the control and treated cohort that were determined by bulk techniques (AAS) and microprobe techniques were the same, within experimental error, provides strong evidence for a lack of bias in the selection procedure for single-cell analysis. Student's *t*-tests were performed to determine changes between paired data sets with Welch's correction employed for unequal variances. Significance was accepted at the 95% confidence interval ($P < 0.05$).

RESULTS

H_2O_2 Affects the Cytosolic Elemental Distribution and Membrane Integrity in Cultured PAEC. A comparison of the intracellular distributions of the elements within control PAEC and cells treated with 50 μM H_2O_2 afforded a global overview of the changes in intracellular elemental content and distribution induced by exposure of cultured PAEC to a low pathophysiologic concentration of the oxidant. The representative elemental maps that are shown in Figure 1 indicate a general trend for cellular-ion efflux. Furthermore, with the exception of Fe, elemental maps obtained from the two treatment groups also showed a general trend for an increased level of localization of K (not shown), Ca, and the trace metals in the region of the cell defined by the areas of high intensities in the phosphorus (DNA) and zinc (Zn finger proteins) maps (Figure 1), which defines the nucleus (*44*), indicating that the loss of these elements occurs mainly from the cytoplasm (cf., elemental maps in Figure 1). While there was little change to the elemental content of the nucleus, the overall volume-normalized elemental density decreased significantly for P, K, Ca, Cr, Fe, Ni, Cu, and Zn in the H_2O_2-treated cells compared to control cells, and

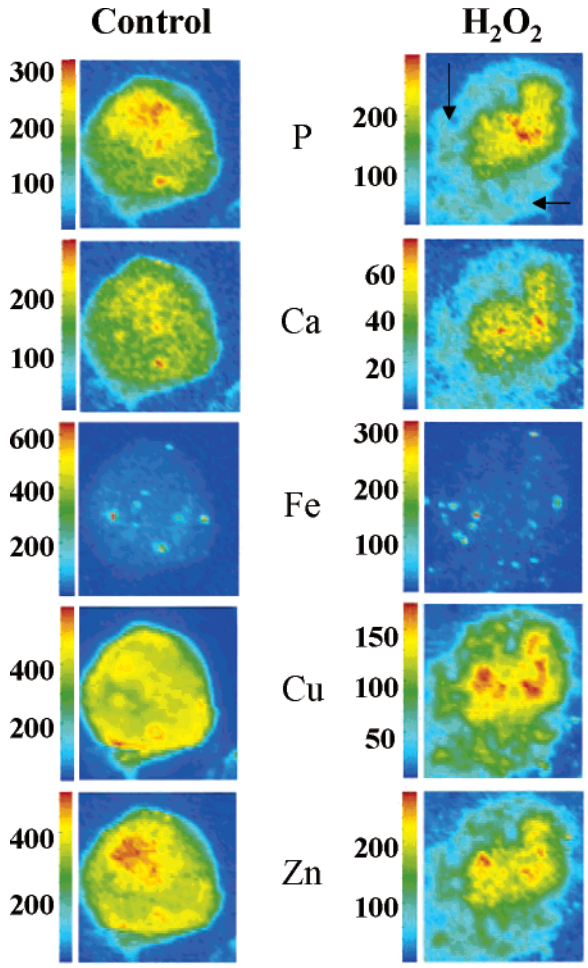

FIGURE 1: Elemental distribution in cultured PAEC before and after treatment with H_2O_2. Confluent PAEC were equilibrated in HEPES-buffered PSS and treated with HEPES-buffered PSS alone (Control) or HEPES-buffered PSS containing 50 μM reagent H_2O_2 (treatment) for 30 min, and the intracellular contents of a range of elements (including P, S, Cl, K, Ca, Cr, Fe, Ni, Cu, and Zn) were determined by hard X-ray ion mapping as described in Materials and Methods. Elemental maps are shown for P, Ca, Fe, Cu, and Zn (S, Cl, and K maps and the X-ray scatter are shown in the Supporting Information). Data are representative of maps obtained from at least three independent cells. Arrows on the P map of the H_2O_2-treated cells indicate regions of blebbing. Comparisons between individual ion maps require careful evaluation of the corresponding color-graduated density bars. Absolute elemental concentrations were not determined in these experiments but were determined from the GFAAS experiments. Areas of high density of P and Zn are indicative of the cell nucleus (*44*). Note the relative change in the elemental distribution that occurs after exposure to H_2O_2 is largely localized to the cytoplasm, while the elemental distribution at the nucleus remains largely unchanged. Data are representative of four samples from the H_2O_2 treatment group or three samples from the corresponding controls. The scan areas are 15 μm $\times$ 15 μm for the control and 15 μm $\times$ 18 μm for the treated cell.

although the content of S and Cl in PAEC also decreased, this was not significant (Table 1). Importantly, the average cell radius did not differ significantly between treatment groups, indicating that changes in the intracellular elemental concentration rather than cell volume are responsible for the decreased size-normalized elemental content (Table 1).

The SRIXE results showed that H_2O_2-treated cells were invariably less regular in shape than the control cells (Figure 1). In addition, membrane blebbing was observed in the treated cells. These observations indicate that H_2O_2 induced damage to the cell membrane, and the SRIXE results showed that large changes also occurred in the cytoplasm.

Independent Verification of the Elemental Concentrations in PAEC. To confirm the trends established by the SRIXE microprobe studies, a series of elemental analyses were performed on control and H_2O_2-treated PAEC. Thus, the concentrations of the elements Cu, Zn, and Fe in bulk cells were determined by GFAAS in whole cell lysates obtained from control and oxidant-treated PAEC (Table 2). Consistent with the SRIXE data, the concentration of all three elements decreased significantly in the H_2O_2-treated cells. Estimates of changes to intracellular Cu (4.3-fold), Zn (3.1-fold), and Fe (3.3-fold) levels with SRIXE expressed as a fold decrease relative to the corresponding control were within the experimental error of those determined by GFAAS for Cu (4.5-fold), Zn (2.5-fold), and Fe (1.5-fold), thereby verifying that the individual cell analyses were representative of bulk cells, at least for these elements.

The intracellular contents of GSH and GSSG were determined in cultured PAEC before and after they were treated with H_2O_2 (Figure 2). The GSH content decreased slightly ($\sim$25%), but significantly, after treatment with 50 μM H_2O_2, while the intracellular GSSG content was unchanged between control and H_2O_2-treated PAEC. The glutathione redox status [measured as the [GSSG]/([GSH] + [GSSG]) ratio] was not significantly different between treatment groups. As GSH represents a major source of sulfur-containing molecules within cells, a decrease in S content amounting to $\sim$25% of the total cellular GSH alone may be taken as support for the SRIXE data that also showed a decreased intracellular S content in H_2O_2-treated PAEC ($\sim$40%); albeit, this was not statistically significant due to the large variation in S content. Furthermore, our calculated loss of intracellular GSH content is consistent with that from an independent report indicating a similar loss of GSH content from bovine pulmonary artery endothelial cells exposed to H_2O_2 (*45*).

Next, the calcium concentration in PAEC before and immediately after H_2O_2 treatment was indirectly assessed by subsequently treating the confluent PAEC with the fluorescent probe INDO-1 and assessing changes in the fluorescence of the cell population with flow cytometry, as shown in Figure 3A. Consistent with data reported previously (*19*), the intracellular free Ca^{2+} level increased 3-fold relative to that of control cells after cells were exposed to 50 μM H_2O_2 (Figure 3B). These data for the bulk cells conflict directly with the efflux of Ca^{2+} ions determined by hard SRIXE mapping of individual cells, although it is uncertain whether this is due to an artifact of the technique employing the Ca^{2+} probe or the SRIXE results (see the Discussion).

To address the conflicting data for $[Ca^{2+}]_i$ determined by SRIXE mapping versus the Ca^{2+} probe combined with flow cytometry, additional studies were performed with FLUO-3AM as a second independent Ca^{2+} probe and at times that closely matched the time frame required for preparation of PAEC samples for SRIXE mapping as shown in Figure 4. After a 30 or 60 min incubation with added H_2O_2 (final concentration of 50 μM) followed by a 60 min incubation in the presence of FLUO-3AM, and subsequent de-esterification of the probe (following the manufacturer's instructions), $[Ca^{2+}]_i$ increased time-dependently and remained

Table 1: Volume-Normalized Elemental Content within Porcine Aortic Endothelial Cells before and after Treatment with Reagent H_2O_2[a]

	elemental content of cells (arbitrary units)										radius
treatment	P	S	Cl	K	Ca	Cr	Fe	Ni	Cu	Zn	(μm)
control	0.61 (0.16)	0.76 (0.16)	7.42 (1.32)	1.70 (0.29)	0.36 (0.09)	0.23 (0.08)	0.19 (0.106)	0.21 (0.09)	18.34 (7.54)	1.29 (0.40)	6.63 (0.25)
H_2O_2-treated	0.37 (0.09)	0.46 (0.19)	5.04 (2.82)	0.35 (0.20)	0.09 (0.05)	0.05 (0.04)	0.06 (0.03)	0.03 (0.02)	3.99 (1.17)	0.52 (0.18)	6.67 (0.29)
P value	0.04	0.06	0.18	0.0001	0.002	0.006	0.007	0.007	0.009	0.01	0.63
ratio	1.6	1.7	1.5	4.9	4.0	4.6	3.2	7.0	4.6	2.5	1.0

[a] The relative intracellular elemental content was obtained by SRIXE microprobe studies as outlined in Materials and Methods. Confluent PAEC ($\sim 1 \times 10^6$ cells) were treated with or without added H_2O_2 (final concentration of 50 μM) and worked up for XAS studies within 2 h of treatment, prior to being freeze-dried. Individual elemental contents were determined and normalized against the corresponding cell volume using the cell radius determined from each individual cell. Data represent the mean (standard deviation) from four (control) or three (H_2O_2-treated) data sets. Statistical significance was accepted at the 95% confidence interval with *P* values determined by a Student's *t*-test using Welch's correction for unequal variances where appropriate. The relative elemental contents cannot be compared between elements.

Table 2: Metal-Ion Concentration in PAEC before and after Treatment with Reagent H_2O_2[a]

treatment	Zn	Cu	Fe
control	33.9 (10.4)	33.6 (5.8)	84.3 (0.2)
H_2O_2-treated	11.0 (2.9)[b]	7.8 (2.2)[b]	56.4 (10.4)[b]

[a] Intracellular ion concentrations were obtained by AAS as outlined in Materials and Methods and expressed in units of parts per billion per milligram of cell protein and corrected for any dilutions of the raw lysate. Confluent PAEC ($\sim 1 \times 10^6$ cells) were treated with or without added H_2O_2 (final concentration of 50 μM) and worked up for AAS studies within a 2-hr period post-treatment. Cellular concentrations of individual ions were normalized against the corresponding total cell protein determined from each individual preparation. The total cell protein did not differ significantly between treatment groups. Data represent the mean (standard deviation) from four control or H_2O_2-treated data sets. [b] Significantly different from the corresponding control ($P < 0.05$).

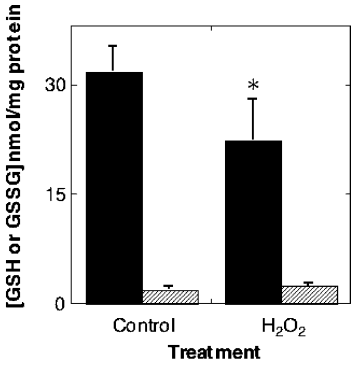

FIGURE 2: Intracellular GSH concentration decreases in cultured PAEC after exposure to H_2O_2. PAEC (1×10^6 cells/well) were washed with HEPES-buffered PSS and then treated with vehicle alone (control) or H_2O_2 (final concentration of 50 μM). After 60 min, the PAEC were harvested and lysed by repeated freezing and thawing, and the intracellular contents of reduced glutathione (GSH, black bars) and oxidized glutathione (GSSG, hatched bars) were measured as described in Materials and Methods. Data represent means ± the standard deviation for four independent preparations of cultured PAEC. The asterisk indicates the value is significantly different from that of corresponding control cells ($P = 0.045$).

elevated relative to the control value (vehicle alone) for the period that was monitored (Figure 4). Thus, the results obtained with FLUO-3AM resembled those obtained with INDO-1.

Finally, the extent of apoptosis and necrosis was determined in PAEC in the absence (control) and presence of 50 μM H_2O_2 (Figure 5). These studies were performed over a time frame that matched the time period spanning harvest and transport of the cells prior to processing for SRIXE

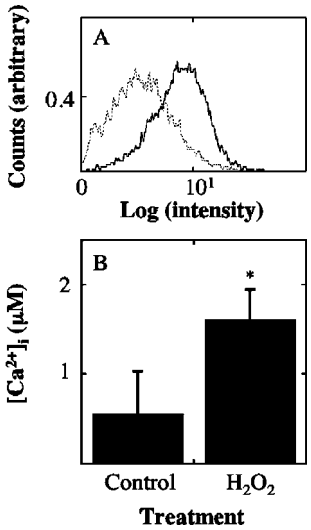

FIGURE 3: H_2O_2-mediated changes in calcium concentration in cultured PAEC. Confluent PAEC ($\sim 1 \times 10^6$ cells) were treated with HEPES-buffered PSS (···) or HEPES-buffered PSS containing 50 μM reagent H_2O_2 (—) for 60 min, and the intracellular content of Ca^{2+} ions was determined by flow cytometry with INDO-1 as described in Materials and Methods. Fluorescence was measured in treated and untreated cells with (A) emission at 405 nm, representing the level of INDO-1-bound intracellular Ca^{2+}. The total $[Ca]_i$ (B) was then determined using published methods (*73*). Note that the time taken from treatment to sample workup includes a 60 min incubation period with added H_2O_2, and then a 90 min preparation time before the cells were ready for analysis. Data represent the means ± the standard deviation for three independent analyses using different PAEC preparations. The asterisk indicates the value is significantly different from that of the corresponding control ($P < 0.05$).

analyses. Under these conditions, both the extent of annexin V binding (apoptosis) and PI staining (necrosis) increased marginally from ~4% in the control cells to ~7% in the peroxide-treated cells after incubation for 1 h at 37 °C. No further increase in the level of annexin V binding or PI staining was determined after incubation for a further 5 h. These data show that there is a small initial increase in the level of cell death following insult, but subsequently, the remaining cells (~85−90%) continue to be viable in the short (1 h) or longer term (6 h).

DISCUSSION

Application of submicrometer-resolution hard X-ray fluorescence elemental distribution mapping to PAEC has provided data on the global changes for intracellular elemental density within these vascular cells and shows for the first

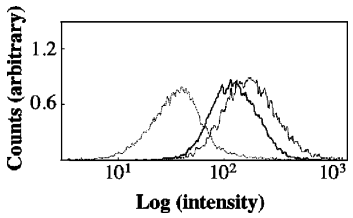

FIGURE 4: H_2O_2-mediated changes in calcium concentration in cultured PAEC. Confluent PAEC (~1 × 10^6 cells) were treated as described in the legend of Figure 3, and the intracellular content of Ca^{2+} ions was determined by flow cytometry with FLUO-3AM as described in Materials and Methods. Fluorescence was measured in the control (•••) and H_2O_2-treated PAEC after 120 (—) and 150 min (- - -) with emission at 525 nm representing the level of FLUO-3AM-bound intracellular Ca^{2+}. Note that the time points selected include a 30 or 60 min incubation period with 50 μM H_2O_2, followed by a 60 min incubation period with the fluorescent probe, and then a 30 min incubation period in the presence of media prior to analysis with flow cytometry. Data are representative of three independent analyses using different preparations of cultured PAEC.

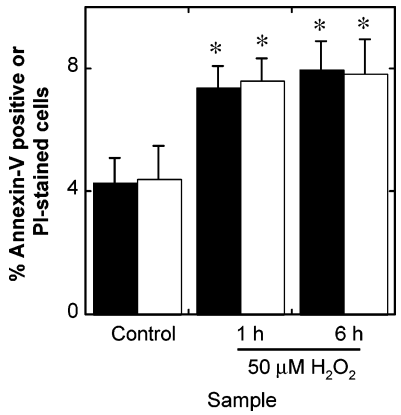

FIGURE 5: Treatment of PAEC with H_2O_2 marginally increases the level of apoptosis and necrosis. Confluent PAEC were incubated for 60 min in HEPES-buffered PSS alone (Control), for 60 min in HEPES-buffered PSS containing 50 μM reagent H_2O_2, or for 60 min in HEPES-buffered PSS containing 50 μM reagent H_2O_2 followed by a further 5 h incubation in complete media. The preparations were then cultured for a further 1 or 6 h at 37 °C, and the extent of annexin V binding (black bars) or propidium iodide (PI) staining (white bars) were determined with a commercial kit and using flow cytometry. Annexin V binding and propidium iodide (PI) staining represent surrogate markers for apoptosis and necrosis, respectively. Data represent the means ± the standard deviation for six independent analyses using different PAEC preparations. Asterisks indicate the value is significantly different from that of the corresponding control ($P < 0.05$).

time a general efflux of metals and phosphorus-containing molecules from the cytoplasm after exposure to (patho)-physiologic concentrations of H_2O_2. It is noteworthy that mitochondria are cytosolic organelles, and therefore, changes to the cytosolic content of ions within the endothelial cells may well reflect changes in the ion content of the mitochondria. The observation that both S and P contents of the cytosol were decreased may then be interpreted as damage to the mitochondrial DNA, which is more extensive and persists longer than nuclear DNA damage. Additionally, the SRIXE data show that the H_2O_2-treated cells are irregularly shaped and exhibit blebbing. These morphological changes are indicative of damage to the cell membrane that may promote membrane permeability (*46*) without a marked decrease in cell viability as judged by the small overall change in the extent of apoptosis and necrosis. Taken

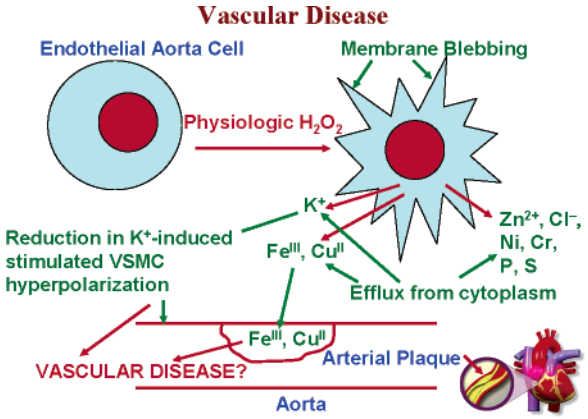

FIGURE 6: Schematic of the changes occurring when endothelial aorta cells are exposed to pathophysiological concentrations of hydrogen peroxide under conditions of oxidative stress.

together, the SRIXE results show, for the first time, that H_2O_2-induced damage is restricted mainly to the cell membrane and cytoplasm of PAEC rather than the cell nucleus, as judged by the observed changes to membrane and cytoplasmic components. The SRIXE results also provide a potential mechanism for cell detoxification due to the efflux of metal ions, which result from the initial H_2O_2-mediated changes to cell membrane and cytosol composition. Such an efflux potentially limits further damaging intracellular metal-mediated redox chemistry with H_2O_2 through Fenton-like chemistry that enhances production of reactive oxygen species. They may also explain the increased levels of such ions in arterial plaques, whether or not they are involved in the formation of the plaque. Overall, the SRIXE experiments offer evidence to support the notion that endothelial cells exposed to H_2O_2 in culture are susceptible to enhanced mobilization of cellular metal ions mainly from the cell cytoplasm into the extracellular space. The changes to the cells are summarized in the scheme depicted in Figure 6. It is important to note, however, that the observed elemental efflux from the cytoplasm is not just due to damage in the cell membrane as the ratio of elemental content in the control versus treated cells varies depending on the element. Moreover, even for a given element, such as S, the efflux depends on whether it is GSH (reduction in intracellular content) or GSSG where there is no change. Taken together, this suggests specific transport mechanisms contribute, at least in part, to the elemental efflux.

Modulation of K^+-ion transport activity is emerging as an important determinant of vasomotor function. The effect of oxidative stress on ion transport proteins has been investigated for a variety of cell types. For example, studies that implicate H_2O_2 as a potential hyperpolarizing factor consistently show that the peroxide activates high-, intermediate-, and low-conductance K_{Ca} channels to release K^+ from endothelial cells (*12*, *47*). The K^+ ions released by the endothelium subsequently activate K^+-ion conductance in underlying VSMC that results in vessel hyperpolarization. Also, H_2O_2 stimulates hyperpolarization by stimulating K^+ efflux directly from VSMC (*14*). The SRIXE experiments presented here are important in that they provide direct evidence for the stimulated loss of K^+ from the cytoplasm of endothelial cells, with a 5-fold reduction in total cellular K^+ content under the experimental conditions reported here. Such a reduction in intracellular K^+ content is likely to have

an impact on the ability of endothelial cells to stimulate VSMC hyperpolarization through mechanisms that rely on the stimulated release of K^+ ions (*48*). A recent study investigating the role of K^+-ion conductance in the NO-independent component of the acetylcholine-induced vasodilation is further supportive of this notion (*49*). Therefore, depletion of K^+ ions may explain the loss of vascular function in vessels pretreated with H_2O_2, observed in some (*50*−*52*) though not all studies (*53*).

The SRIXE experiments provide the first direct measurements of the effects of both total elemental content and intracellular elemental distribution in PAEC cells treated with H_2O_2. The cryofixation/freeze-drying process that was employed protects the integrity of the cells (*54*), and it is not subject to artifacts introduced by chemical pretreatments of the cells that can affect the biochemical and functional properties being measured, as is the case for many other techniques. The integrity of the PAEC cells exposed to hydrogen peroxide is further exemplified by the high level of cell viability determined immediately prior to preparation for SRIXE analyses. The SRIXE experiments show that the H_2O_2-treated cells are more irregular and exhibit blebbing compared to the control cells. Such changes in morphology are indicative of damage to the cell membrane, which would promote increased membrane permeability. Although PAEC are adherent cells and, therefore, were harvested with trypsin prior to SRIXE measurements, this removal of the adherent cells from the culture plate itself is not likely to cause cell blebbing, as blebbing was not observed for the control cells. Therefore, our results indicate that the membrane in the H_2O_2-treated cells is more damaged than in the corresponding control cells, taking into account the processing for SRIXE analyses. Taken together with the elemental maps, the SRIXE results show that the damage induced by H_2O_2 under the pathologic conditions that were used is restricted mainly to the outer membrane and the cytoplasm of PAEC. Apparently, H_2O_2 is consumed by reactions with membrane and intracellular components in the cytoplasm before it reaches the nucleus. GSH is a target in the cytoplasm for added H_2O_2, as judged by the modest, though significant, decrease in the cellular GSH level. The SRIXE results are also important as they provide novel data to explain a potential mechanism for cell detoxification of H_2O_2, with possible implications for vascular disease. The efflux of metal ions resulting from an initial H_2O_2 exposure reduces the potential for subsequent damage due to intracellular metal redox chemistry with H_2O_2. Of potential relevance in this context, extracellular fluids are relatively rich in proteins that bind transition metals, thereby rendering them less redox active (*55*). Transition metal efflux from cells during periods of enhanced oxidative stress may explain the presence of Cu and Fe in arterial plaques (*56*, *57*), regardless of whether these metals are directly involved in the formation of these plaques (*58*−*60*).

Apart from the obvious damage to the cell membrane revealed by the SRIXE experiments, which is likely to increase membrane permeability, other more specific mechanisms for metal efflux are possible. The observed decrease in PAEC stores of Zn^{2+} can be readily explained through the known interaction of H_2O_2 with metallothionein in combination with enhanced Zn^{2+} efflux through Zn transporter 1 (*61*). Thus, H_2O_2-induced oxidation of cysteine sulfhydryl groups in metallothionein (*62*) results in the loss of metal binding of the protein (*63*) and promotes the temporal accumulation of cytosolic Zn^{2+} ions. As accumulated zinc may lead to toxicity, cells can protect themselves by inducing Zn^{2+} efflux, as has been reported for Fe^{2+} (*64*). A similar mechanism of intracellular Cu mobilization through redox regulation of copper-bound metallothionein (*65*) may result in the accumulation of intracellular Cu.

In contrast to the known mechanisms for H_2O_2-mediated efflux of K^+ and Zn^{2+} and possibly Cu, such efflux has not been reported previously for Fe, Ni, Cr, S, P, and Cl, although the observed nonspecific damage to the cell membrane would allow for a general ion and molecule efflux. Mobilization of iron is complex with a requirement for Fe acceptors specific for Fe(II) and Fe(III), iron-storage proteins, as well a group of specific transferrin receptors, which are all involved in intra- and extracellular Fe transport (*66*). The expression of the transferrin receptor is dependent on iron-regulatory proteins that are sensitive to cellular redox status (*67*), and treatment of cells with menadione (a source of H_2O_2) affects intracellular copper and iron homeostasis (*68*). Interestingly, the combination of $^{\bullet}NO$ and glucose can stimulate efflux of Fe from cells together with glutathione (*69*). Whether a similar role exists for H_2O_2 in the depletion of cellular Fe levels together with S, possibly through the enhanced efflux of reduced glutathione, remains to be verified. Similarly, a Ca^{2+}-activated chloride channel closely regulates the Cl^- content of endothelial cells (*70*), although it is not clear whether exposure of endothelial cells to H_2O_2 modulates the Cl^--channel function.

The conflicting data presented here for intracellular Ca^{2+} estimated by SRIXE and flow cytometry require some discussion. The strong correlation between the GFAAS and SRIXE determinations for the total cell content for Fe, Cu, and Zn provides evidence that the SRIXE-derived changes in Ca^{2+} content are indeed an accurate reflection of the changes occurring under the treatment conditions. However, one potential artifact in the assessment of Ca^{2+} by SRIXE is the overlap of the Ca fluorescence peak with the much stronger K fluorescence peak; a large reduction in the intracellular K^+ level could conceivably lead to an incorrect observation of a reduced intracellular Ca^{2+} level. The likelihood of similar artifacts occurring in the SRIXE-derived data for elements other than Ca is very much lower as their fluorescence detection windows are better separated from adjacent fluorescence peaks and, therefore, adjacent fluorescence peaks are not as dominant.

In contrast to SRIXE, the use of fluorescence probes is an indirect method that requires chemical modification of the Ca^{2+} environment, which can influence both the mobility and distribution of the element within the cell, and may also lead to an incorrect determination of the intracellular Ca^{2+} level. There are chemical reasons why the fluorescence probes could lead to erroneous results. As shown by the SRIXE experiments, there is considerable membrane damage caused by the H_2O_2 treatment, and this is likely to result in the membrane being more permeable to the fluorescent probe in the treated as opposed to the control cells. Thus, the increase in the magnitude of the fluorescence signal may merely reflect an increase in the concentration of the probe entering the cell. This could also be compounded by the fact that the strong complexes formed between the probe and

Ca^{2+} are likely to prevent, or at least restrict, the efflux mechanisms. In particular, Ca^{2+} release channels contain a number of redox-sensitive sulfhydryl groups (*71*), and their activity can be modulated in response to S-nitrosylation (*72*). Reactive sulfhydryl groups are also susceptible to oxidative modification by H_2O_2 in a reversible process (*73*). Therefore, it is possible that H_2O_2 is capable of modulating reactive thiols in Ca^{2+} channel proteins within endothelial cells to promote Ca^{2+} efflux. In support of this idea, the interaction between Na^+ and H_2O_2 stimulates Ca^{2+} mobilization, resulting in the release of Ca^{2+} from cells transfected with the $(Na^+)Ca^{2+}$ cation exchange transporter (*74*), but such a transporter would have to compete with the strong binding of Ca^{2+} to the fluorescent probe to be effective. Together, these factors may explain the conflicting data obtained in this study between the determination of Ca^{2+} levels by SRIXE and the determination by the use of a fluorescence probe; however, we are unable, at present, to unambiguously determine whether Ca^{2+} levels are elevated or decreased in H_2O_2-treated PAEC, and this area warrants further investigation.

Overall, the results obtained in this study establish that cultured endothelial cells respond to added H_2O_2 with a general decrease in intracellular cytosolic elemental content. This global change in cellular ion content is not associated with a dramatic decrease in cell toxicity, since ~85−90% of the cells remained viable immediately prior to being processed for SRIXE analyses. One limitation of the current study is that cell viability assays could not be performed following cryo-processing. Although morphologically the cells appeared to be unchanged, the possibility that cellular necrosis could occur from this treatment remains; however, the low-temperature freeze-drying process is unlikely to have affected the distribution and concentration of the elements. At present, the precise mechanism(s) for the general efflux of all the elements monitored is not clear, but the modification of membrane structure leading to nonspecific increases in membrane permeability and ion-channel transport proteins are implicated in these processes. Preservation of endothelial cell function is paramount to maintenance of vascular hemostasis, and a dysfunctional endothelium is implicated as an early event in several vascular diseases. Whether the biochemical changes induced in aortic endothelial cells by a relatively low pathophysiologic dose of H_2O_2 are related to the progression of diseases such as diabetes, atherosclerosis, and hypertension is not known at present. Therefore, the general efflux of elemental ions and their potential for involvement in pathological processes warrant further investigation.

ACKNOWLEDGMENT

We thank Dr. Aviva Levina for assistance with GFAAS experiments and for critically reviewing aspects of the manuscript.

SUPPORTING INFORMATION AVAILABLE

Additional SRIXE elemental distribution maps (K, Cl, and S) and X-ray scatter maps. This material is available free of charge via the Internet at http://pubs.acs.org.

REFERENCES

1. Utoguchi, N., Ikeda, K., Saeki, K., Oka, N., Mizuguchi, H., Kubo, K., Nakagawa, S., and Mayumi, T. (1995) Ascorbic acid stimulates barrier function of cultured endothelial cell monolayer, *J. Cell. Physiol. 163*, 393−399.
2. Furchgott, R. F., and Zawadzki, J. V. (1980) The obligatory role of endothelial cells in the relaxation of arterial smooth muscle by acetylcholine, *Nature 288*, 373−376.
3. Ignarro, L. J., Buga, G. M., Wood, K. S., Byrns, R. E., and Chaudhuri, G. (1987) Endothelium-derived relaxing factor produced and released from artery and vein is nitric oxide, *Proc. Natl. Acad. Sci. U.S.A. 84*, 9265−9269.
4. Azuma, H., Ishikawa, M., and Sekizaki, S. (1986) Endothelium-dependent inhibition of platelet aggregation, *Br. J. Pharmacol. 88*, 411−415.
5. Kubes, P., Suzuki, M., and Granger, D. N. (1991) Nitric oxide: An endogenous modulator of leukocyte adhesion, *Proc. Natl. Acad. Sci. U.S.A. 88*, 4651−4655.
6. Tanner, F. C., Meier, P., Greutert, H., Champion, C., Nabel, E. G., and Luscher, T. F. (2000) Nitric oxide modulates expression of cell cycle regulatory proteins: A cytostatic strategy for inhibition of human vascular smooth muscle cell proliferation, *Circulation 101*, 1982−1989.
7. Hollenberg, S. M., Klein, L. W., and Parrillo, J. E. (2001) Nitric oxide modulates expression of cell cycle regulatory proteins: A cytostatic strategy for inhibition of human vascular smooth muscle cell proliferation, *Circulation 104*, 3091−3096.
8. Ludmer, P. L., Selwyn, A. P., Shook, T. L., Wayne, R. R., Mudge, G. H., Alexander, R. W., and Ganz, P. (1986) Paradoxical vasoconstriction induced by acetylcholine in atherosclerotic coronary arteries, *N. Engl. J. Med. 315*, 1046−1051.
9. Kobayashi, T., and Kamata, K. (2002) Modulation by hydrogen peroxide of noradrenaline-induced contraction in aorta from streptozotocin-induced diabetic rat, *Eur. J. Pharmacol. 441*, 83−89.
10. Matsumoto, T., Wakabayashi, K., Kobayashi, T., and Kamata, K. (2004) Alterations in vascular endothelial function in the aorta and mesenteric artery in type II diabetic rats, *Can. J. Physiol. Pharmacol. 82*, 175−182.
11. Panza, J. A., Garcia, C. E., Kilcoyne, C. M., Quyyumi, A. A., and Cannon, R. O., III (1995) Impaired endothelium-dependent vasodilation in patients with essential hypertension. Evidence that nitric oxide abnormality is not localized to a single signal transduction pathway, *Circulation 91*, 1732−1738.
12. Matoba, T., Shimokawa, H., Nakashima, M., Hirakawa, Y., Mukai, Y., Hirano, K., Kanaide, H., and Takeshita, A. (2000) Hydrogen peroxide is an endothelium-derived hyperpolarizing factor in mice, *J. Clin. Invest. 106*, 1521−1530.
13. Fisslthaler, B., Popp, R., Kiss, L., Potente, M., Harder, D. R., Fleming, I., and Busse, R. (1999) Cytochrome P450 2C is an EDHF synthase in coronary arteries, *Nature 401*, 493−497.
14. Edwards, G., Dora, K. A., Gardener, M. J., Garland, C. J., and Weston, A. H. (1998) K^+ is an endothelium-derived hyperpolarizing factor in rat arteries, *Nature 396*, 269−272.
15. Matoba, T., Shimokawa, H., Kubota, H., Kunihiro, I., Urakami-Harasawa, L., Mukai, Y., Hirakawa, Y., Akaike, T., and Takeshita, A. (2003) Electron spin resonance detection of hydrogen peroxide as an endothelium-derived hyperpolarizing factor in porcine coronary microvessels, *Arterioscler. Thromb. Vasc. Biol. 23*, 1224−1230.
16. Chen, K., Thomas, S. R., and Keaney, J. F., Jr. (2003) Beyond LDL oxidation: ROS in vascular signal transduction, *Free Radical Biol. Med. 35*, 117−132.
17. Thomas, S. R., Chen, K., and Keaney, J. F., Jr. (2002) Hydrogen peroxide activates endothelial nitric-oxide synthase through coordinated phosphorylation and dephosphorylation via a phosphoinositide 3-kinase-dependent signaling pathway, *J. Biol. Chem. 277*, 6017−6024.
18. Cai, H., Li, Z., Dikalov, S., Holland, S. M., Hwang, J., Jo, H., Dudley, S. C., Jr., and Harrison, D. G. (2002) NAD(P)H oxidase-derived hydrogen peroxide mediates endothelial nitric oxide production in response to angiotensin II, *J. Biol. Chem. 277*, 48311−48317.
19. Hu, Q., Corda, S., Zweier, J. L., Capogrossi, M. C., and Ziegelstein, R. C. (1998) Hydrogen peroxide induces intracellular calcium oscillations in human aortic endothelial cells, *Circulation 97*, 268−275.
20. Liu, Y., and Gutterman, D. D. (2002) Oxidative stress and potassium channel function, *Clin. Exp. Pharmacol. Physiol. 29*, 305−311.
21. Deshpande, N. N., Sorescu, D., Seshiah, P., Ushio-Fukai, M., Akers, M., Yin, Q., and Griendling, K. K. (2002) Mechanism of

hydrogen peroxide-induced cell cycle arrest in vascular smooth muscle, *Antioxid. Redox Signaling 4*, 845−854.
22. Vasquez-Vivar, J., Kalyanaraman, B., Martasek, P., Hogg, N., Masters, B. S., Karoui, H., Tordo, P., and Pritchard, K. A., Jr. (1998) Superoxide generation by endothelial nitric oxide synthase: The influence of cofactors, *Proc. Natl. Acad. Sci. U.S.A. 95*, 9220−9225.
23. White, C. R., Darley-Usmar, V., Berrington, W. R., McAdams, M., Gore, J. Z., Thompson, J. A., Parks, D. A., Tarpey, M. M., and Freeman, B. A. (1996) Circulating plasma xanthine oxidase contributes to vascular dysfunction in hypercholesterolemic rabbits, *Proc. Natl. Acad. Sci. U.S.A., 93*, 8745−8749.
24. Lui, Y., Zhao, H., Li, H., Kalyanaraman, B., Nicolosi, A. C., and Gutterman, D. D. (2003) Mitochondrial sources of H_2O_2 generation play a key role in flow-mediated dilation in human coronary resistance arteries, *Circ. Res. 93*, 573−580.
25. Fleming, I., Michaelis, U. R., Bredenkotter, D., Fisslthaler, B., Dehghani, F., Brandes, R. P., and Busse, R. (2001) Endothelium-derived hyperpolarizing factor synthase (cytochrome P450 2C9) is a functionally significant source of reactive oxygen species in coronary arteries, *Circ. Res. 88*, 44−51.
26. McNally, J. S., Davis, M. E., Giddens, D. P., Saha, A., Hwang, J., Dikalov, S., Jo, H., and Harrison, D. G. (2003) Role of xanthine oxidoreductase and NAD(P)H oxidase in endothelial superoxide production in response to oscillatory shear stress, *Am. J. Physiol. 285*, H2290−H2297.
27. Rajagopalan, S., Kurz, S., Munzel, T., Tarpey, M., Freeman, B. A., Griendling, K. K., and Harrison, D. G. (1996) Angiotensin II-mediated hypertension in the rat increases vascular superoxide production via membrane NADH/NADPH oxidase activation. Contribution to alterations of vasomotor tone, *J. Clin. Invest. 97*, 1916−1923.
28. Beckman, J. S., Beckman, T. W., Chen, J., Marshall, P. A., and Freeman, B. A. (1990) Apparent hydroxyl radical production by peroxynitrite: Implications for endothelial injury from nitric oxide and superoxide, *Proc. Natl. Acad. Sci. U.S.A. 87*, 1620−1624.
29. Zou, M. H., Shi, C., and Cohen, R. A. (2002) Oxidation of the zinc-thiolate complex and uncoupling of endothelial nitric oxide synthase by peroxynitrite, *J. Clin. Invest. 109*, 817−826.
30. Landmesser, U., Dikalov, S., Price, S. R., McCann, L., Fukai, T., Holland, S. M., Mitch, W. E., and Harrison, D. G. (2003) Oxidation of tetrahydrobiopterin leads to uncoupling of endothelial cell nitric oxide synthase in hypertension, *J. Clin. Invest. 111*, 1201−1209.
31. Stone, J. R. (2004) An assessment of proposed mechanisms for sensing hydrogen peroxide in mammalian systems, *Arch. Biochem. Biophys. 422*, 119−124.
32. Liu, X., and Zweier, J. L. (2001) A real-time electrochemical technique for measurement of cellular hydrogen peroxide generation and consumption: Evaluation in human polymorphonuclear leukocytes, *Free Radical Biol. Med. 31*, 894−901.
33. Zobali, F., Besler, T., Ari, N., and Karasu, I. (2002) Hydrogen peroxide-induced inhibition of vasomotor activity: Evaluation of single and combined treatments with vitamin A and insulin in streptozotocin-diabetic rats, *Exp. Diabesity Res. 3*, 119−130.
34. Karasu, C. (2000) Time course of changes in endothelium-dependent and -independent relaxation of chronically diabetic aorta: Role of reactive oxygen species, *Eur. J. Pharmacol. 392*, 163−173.
35. Lacy, F., O'Connor, D. T., and Schmid-Schoenbein, G. W. (1998) Plasma hydrogen peroxide production in hypertensive and normotensive subjects at genetic risk of hypertension, *J. Hypertens. 16*, 291−303.
36. Heitzer, T., Schlinzig, T., Krohn, K., Meinertz, T., and Munzel, T. (2001) Endothelial cell dysfunction, oxidative stress, and risk of cardiovascular events in patients with coronary artery disease, *Circulation 104*, 2673−2678.
37. Dillon, C. T., Lay, P. A., Bonin, A. M., Cholewa, M., Legge, G. J. F., Collins, T. J., and Kostka, K. L. (1998) Permeability, cytotoxicity, and genotoxicity of chromium(V) and chromium(VI) complexes in V79 Chinese hamster lung cells, *Chem. Res. Toxicol. 11*, 119−129.
38. Cholewa, M., Turnbull, I. F., Legge, G. J. F., Weigold, H., Marcuccio, S. M., Holan, G., Tomlinson, E., Wright, P. J., Dillon, C. T., Lay, P. A., and Bonin, A. M. (1995) Investigation of the uptake of drugs, carcinogens and mutagens by individual mammalian cells using a scanning proton microprobe, *Nucl. Instrum. Methods Phys. Res., Sect. B 104*, 317−323.
39. Cai, Z., Lai, B., Yun, W., Ilinski, P., Legnini, D., Maser, J., and Rodrigues, W. (2000) A hard X-ray scanning microprobe for fluorescence imaging and micro-diffraction at the Advanced Photon Source, *Am. Inst. Phys. Proc. 507* (X-ray Microscopy VI), 472−477.
40. Yun, W., Lai, B., Cai, Z., Maser, J., Legnini, D., Gluskin, E., Chen, Z., Krasnoperova, A. A., Vladimirsky, Y., Cerrina, F., Di Fabrizio, E., and Gentili, M. (1999) Nanometer focusing of hard X-rays by phase zone plates, *Rev. Sci. Instrum. 70*, 2238−2241.
41. Lee, H.-R., Lai, B., Yun, W., Mancini, D., and Cai, Z. (1997) X-ray microtomography as a fast three-dimensional imaging technology using a CCD camera coupled with a $CdWO_4$ single-crystal scintillator, *Proc. SPIE-Int. Soc. Opt. Eng. 3149*, 257−264.
42. Takahashi, A., Camacho, P., Lechleiter, J. D., and Herman, B. (1999) Measurement of intracellular calcium, *Physiol. Rev. 79*, 1089−1125.
43. Dillon, C. T., Lay, P. A., Bonin, A. M., Cholewa, M., and Legge, G. J. (2000) Permeability, cytotoxicity, and genotoxicity of Cr(III) complexes and some Cr(V) analogues in V79 Chinese hamster lung cells, *Chem. Res. Toxicol. 13*, 742−748.
44. Dillon, C. T., Lay, P. A., Kennedy, B. J., Stampfl, A. P. J., Cai, Z. H., Ilinski, P., Rodrigues, W., Legnini, D. G., Lai, B., and Maser, J. (2002) Hard X-ray microprobe studies of chromium-(VI)-treated V79 Chinese hamster lung cells: Intracellular mapping of the biotransformation products of a chromium carcinogen, *J. Biol. Inorg. Chem. 7*, 640−645.
45. McAmis, W. C., Schaeffer, R. C., Jr., Baynes, J. W., and Wolf, M. B. (2003) Menadione causes endothelial barrier failure by a direct effect on intracellular thiols, independent of reactive oxidant production, *Biochim. Biophys. Acta 1641*, 43−53.
46. Nusbaum, P., Laine, C., Seveau, S., Lesavre, P., and Halbwachs-Mecarelli, L. (2004) Early membrane events in polymorphonuclear cell (PMN) apoptosis: Membrane blebbing and vesicle release, CD43 and CD16 down-regulation and phosphatidylserine externalization, *Biochem. Soc. Trans. 32*, 477−479.
47. Shimokawa, H., and Matoba, T. (2004) Hydrogen peroxide as an endothelium-derived hyperpolarizing factor, *Pharmacol. Res. 49*, 543−549.
48. Schuster, A., Beny, J.-L., and Meister, J.-J. (2003) Modelling the electrophysiological endothelial cell response to bradykinin, *Eur. Biophys. J. 32*, 370−380.
49. Dabisch, P. A., Liles, J. T., Taylor, J. T., Sears, B. W., Saenz, R., and Kadowitz, P. J. (2004) Role of potassium channels in the nitric oxide-independent vasodilator response to acetylcholine, *Pharmacol. Res. 49*, 207−215.
50. Mian, K. B., and Martin, W. (1997) Hydrogen peroxide-induced impairment of reactivity in rat isolated aorta: Potentiation by 3-amino-1,2,4-triazole, *Br. J. Pharmacol. 121*, 813−819.
51. Harrison, G. J., Jordan, L. R., and Willis, R. J. (1994) Deleterious effects of hydrogen peroxide on the function and ultrastructure of cardiac muscle and the coronary vasculature of perfused rat hearts, *Can. J. Cardiol. 10*, 843−849.
52. Wei, E. P., and Kontos, H. A. (1990) H_2O_2 and endothelium-dependent cerebral arteriolar dilation. Implications for the identity of endothelium-derived relaxing factor generated by acetylcholine, *Hypertension 16*, 162−169.
53. Kobayashi, T., and Kamata, K. (2002) Modulation by hydrogen peroxide of noradrenaline-induced contraction in aorta from streptozotocin-induced diabetic rat, *Eur. J. Pharmacol. 441*, 83−89.
54. Zierold, K. (1992) Comparison of cryopreparation techniques for electron probe microanalysis of cells as exemplified by human erythrocytes, *Scanning Microsc. 6*, 1137−1145.
55. Stocker, R., and Keaney, J. F., Jr. (2004) Role of oxidative modifications in atherosclerosis, *Physiol. Rev. 84*, 1381−1478.
56. Stadler, N., Lindner, R. A., and Davies, M. J. (2004) Direct detection and quantification of transition metal ions in human atherosclerotic plaques: Evidence for the presence of elevated levels of iron and copper, *Arterioscler. Thromb. Vasc. Biol. 24*, 949−954.
57. Lamb, D. J., Mitchinson, M. J., and Leake, D. S. (1995) Transition metal ions within human atherosclerotic lesions can catalyse the oxidation of low-density lipoprotein by macrophages, *FEBS Lett. 374*, 12−16.
58. Monnier, V. M. (2001) Transition metals redox: Reviving an old plot for diabetic vascular disease, *J. Clin. Invest. 107*, 799−801.
59. Corti, M. C., Gaziano, M., and Hennekens, C. H. (1997) Iron status and risk of cardiovascular disease, *Ann. Epidemiol. 7*, 62−68.

60. Darley-Usmar, V., and Halliwell, B. (1996) Blood radicals: Reactive nitrogen species, reactive oxygen species, transition metal ions, and the vascular system, *Pharm. Res. 13*, 649−662.
61. Palmiter, R. D. (2004) Protection against zinc toxicity by metallothionein and zinc transporter 1, *Proc. Natl. Acad. Sci. U.S.A. 101*, 4918−4923.
62. Quesada, A. R., Byrnes, R. W., Krezoski, S. O., and Petering, D. H. (1996) Direct reaction of H_2O_2 with sulfhydryl groups in HL-60 cells: Zinc-metallothionein and other sites, *Arch. Biochem. Biophys. 334*, 241−250.
63. Jimenez, I., Gotteland, M., Zarzuelo, A., Uauy, R., and Speisky, H. (1997) Loss of the metal binding properties of metallothionein induced by hydrogen peroxide and free radicals, *Toxicology 120*, 37−46.
64. Ferris, C. D., Jaffrey, S. R., Sawa, A., Takahashi, M., Brady, S. D., Barrow, R. K., Tysoe, S. A., Wolosker, H., Baranano, D. E., Dore, S., Poss, K. D., and Snyder, S. H. (1999) Haem oxygenase-1 prevents cell death by regulating cellular iron, *Nat. Cell Biol. 1*, 152−157.
65. Fabisiak, J. P., Tyurin, V. A., Tyurina, Y. Y., Borisenko, G. G., Korotaeva, A., Pitt, B. R., Lazo, J. S., and Kagan, V. E. (1999) Redox regulation of copper-metallothionein, *Arch. Biochem. Biophys. 363*, 171−181.
66. Richardson, D. R. (2003) The role of hypoxia and nitrogen monoxide in the regulation of cellular iron metabolism, *J. Lab. Clin. Med. 141*, 289−291.
67. Pantopoulos, K., Weiss, G., and Hentze, M. W. (1996) Nitric oxide and oxidative stress (H_2O_2) control mammalian iron metabolism by different pathways, *Mol. Cell. Biol. 16*, 3781−3788.
68. Calderaro, M., Martins, E. A., and Meneghini, R. (1993) Oxidative stress by menadione affects cellular copper and iron homeostasis, *Mol. Cell. Biochem. 126*, 17−23.
69. Watts, R. N., and Richardson, D. R. (2001) Nitrogen monoxide (NO) and glucose: Unexpected links between energy metabolism and NO-mediated iron mobilization from cells, *J. Biol. Chem. 276*, 4724−4732.
70. Elble, R. C., Widom, J., Gruber, A. D., Abdel-Ghany, M., Levine, R., Goodwin, A., Cheng, H. C., and Pauli, B. U. (1997) Cloning and characterization of lung-endothelial cell adhesion molecule-1 suggest it is an endothelial chloride channel, *J. Biol. Chem. 272*, 27853−27861.
71. Sun, J., Xu, L., Eu, J. P., Stamler, J. S., and Meissner, G. (2001) Classes of thiols that influence the activity of the skeletal muscle calcium release channel, *J. Biol. Chem. 276*, 15625−15630.
72. Sun, J., Xin, C., Eu, J. P., Stamler, J. S., and Meissner, G. (2001) Cysteine-3635 is responsible for skeletal muscle ryanodine receptor modulation by NO, *Proc. Natl. Acad. Sci. U.S.A. 98*, 11158−11162.
73. Claiborne, A., Miller, H., Parsonage, D., and Ross, R. P. (1993) Protein-sulfenic acid stabilization and function in enzyme catalysis and gene regulation, *FASEB J. 7*, 1483−1490.
74. Fang, Y., Rong, M., and He, L. (1997) Interactions of Na^+, H_2O_2 and the Na^+−Ca^{2+} exchanger stimulate Ca^{2+} release in CK1.4 cells, *Clin. Exp. Pharmacol. Physiol. 24*, 170−174.

BI0604375